Temperature- and Hydration-Dependent Protein Dynamics in Photosystem II of Green Plants Studied by Quasielastic Neutron Scattering[†]

Jörg Pieper,*[,‡] Thomas Hauss,[§] Alexandra Buchsteiner,[||] Krzysztof Baczyński,[⊥] Karolina Adamiak,[⊥] Ruep E. Lechner,[§] and Gernot Renger[‡]

Max-Volmer-Laboratories for Biophysical Chemistry, Technische Universität Berlin, Strasse des 17. Juni 135, 10623 Berlin, Germany, Darmstadt University of Technology, Petersenstrasse 22, 64287 Darmstadt, Germany, Hahn-Meitner-Institut Berlin, Glienicker Strasse 100, 14109 Berlin, Germany, and Adam Mickiewicz University, Umultowska 85, 61-614 Poznan, Poland

Received January 31, 2007; Revised Manuscript Received May 11, 2007

ABSTRACT: Protein dynamics in hydrated and vacuum-dried photosystem II (PS II) membrane fragments from spinach has been investigated by quasielastic neutron scattering (QENS) in the temperature range between 5 and 300 K. Three distinct temperature ranges can be clearly distinguished by active type(s) of protein dynamics: (A) At low temperatures ($T < 120$ K), the protein dynamics of both dry and hydrated PS II is characterized by harmonic vibrational motions. (B) In the intermediate temperature range ($120 < T < 240$ K), the total mean square displacement $\langle u^2 \rangle_{total}$ slightly deviates from the predicted linear behavior. The QENS data indicate that this deviation, which is virtually independent of the extent of hydration, is due to a partial onset of diffusive protein motions. (C) At temperatures above 240 K, the protein flexibility drastically changes because of the onset of diffusive (large-amplitude) protein motions. This dynamical transition is clearly hydration-dependent since it is strongly suppressed in dry PS II. The thermally activated onset of protein flexibility as monitored by QENS is found to be strictly correlated with the temperature-dependent increase of the electron transport efficiency from Q_A^- to Q_B (Garbers et al. (1998) *Biochemistry 37*, 11399−11404). Analogously, the freezing of protein mobility by dehydration in dry PS II appears to be responsible for the blockage of Q_A^- reoxidation by Q_B at hydration values lower than 45% r.h. (Kaminskaya et al. (2003) *Biochemistry 42*, 8119−8132). Similar effects were observed for reactions of the water-oxidizing complex as outlined in the Discussion section.

The unique physical properties of proteins provide the basis for optimization and regulatory control of their particular biological function. One prominent example is the electron transfer in Photosystem II (PS II[1]) of oxygen-evolving photosynthetic organisms. PS II is a multimeric protein complex that is embedded into the thylakoid membrane and functions as light-driven water−plastoquinone oxidoreductase (*1*). The light-induced charge separation in PS II leads to the formation of the ion radical pair $P680^{+\bullet}$ $Pheo^{-\bullet}$ (see ref *2* and references therein) followed by stabilization via electron transfer from $Pheo^{-\bullet}$ to a permanently bound plastoquinone 9 (PQ9) molecule Q_A with a time constant of about 300 ps (*3*). Subsequently, plastoquinol PQH_2 is formed at the acceptor side with Q_A^- acting as reductant. This process comprises two sequential one-electron steps from Q_A^- to a PQ9 molecule transiently bound at the Q_B-site and coupled proton uptake reactions (for a review see ref *4*). The cation radical $P680^{+\bullet}$ provides the driving force for oxidative water splitting into molecular oxygen and four protons that takes place at a manganese-containing water-oxidizing complex (WOC) through a four step reaction sequence referred to as Kok-cycle (*5*). All cofactors participating in these reaction sequences are bound to a heterodimeric protein matrix consisting of polypeptides D1 and D2. Recent X-ray crystallographic studies at resolutions of 3.5 Å (*6*) and 3.0 Å (*7*) have revealed the spatial arrangement of most of these cofactors.

The individual electron-transfer steps in the PS II RC exhibit quite different dependences on temperature. The light-induced $P680^{+\bullet}$ $Q_A^{-\bullet}$ formation remains active at low temperatures (*8*), whereas the subsequent reactions of plastoquinol formation and oxidative water splitting are inhibited below characteristic threshold temperatures. The reoxidation of Q_A^- by Q_B becomes completely blocked at 200 K (*9*−*11*). Interestingly, the transfer step from $Q_A^{-\bullet}$ to $Q_B^{-\bullet}$ is less affected by temperature decrease, as was found in experiments using samples frozen after preillumination with one saturating laser flash at room temperature (*12*). The stepwise oxidation of the WOC by the tyrosine Y_Z^{OX} is also sensitive

[†] Financial support by Deutsche Forschungsgemeinschaft (SFB 429, TP A1) is gratefully acknowledged.

* Corresponding author. Tel: +49-30-31427782. Fax: +49-30-31421122. E-mail: joerg.pieper@tu-berlin.de.

[‡] Technische Universität Berlin.

[§] Darmstadt University of Technology.

[||] Hahn-Meitner-Institut Berlin.

[⊥] Adam Mickiewicz University.

[1] Abbreviations: QENS, quasielastic neutron scattering; PS II, Photosystem II; WOC, water oxidizing complex; FTIR, Fourier transform infrared; SANS, small angle neutron scattering; r.h., relative humidity; MES, 2-[*N*-morpholino]ethanesulfonic acid; Pheo, pheophytin; Chl, chlorophyll; HWHM, half-width at half maximum; FWHM, full-width at half maximum; EISF, elastic incoherent structure factor; QISF, quasielastic incoherent structure factor; DHO, damped harmonic oscillator; LHC II, light-harvesting complex II.

10.1021/bi700179s CCC: $37.00
Published on Web 09/15/2007

to freezing, with characteristic temperatures that depend on the redox state S_i (*13*−*15*). The thermal activation of essential electron transport reactions indicates that protein dynamics is of key relevance for PS II functionality.

The flexibility of proteins depends not only on thermal activation but also on the respective environment and in particular on the presence of hydration water molecules. In a recent study, the effect of dehydration on the light-induced reaction of PS II has been analyzed in films of PS II membrane fragments from spinach. It was shown that lowering of the water content causes an effect similar to freezing, that is, suppression of $Q_A^{-\bullet}$ reoxidation by Q_B and significant modification of the reaction pattern of the PS II donor side (*16*). Likewise, FTIR measurements revealed that S_i-state transitions in the WOC are blocked upon dehydration (*17*). The effect of dehydration has also been studied in anoxygenic purple bacteria. It was shown that in dehydrated samples the electron transfer from Q_A to Q_B (Q_B^-) is impaired (*18*, *19*) and the rate of recombination between $P^{+\bullet}$ and $Q_A^{-\bullet}$ significantly increased (*18*). The recombination reaction between $P^{+\bullet}$ and $Q_A^{-\bullet}$ is also sensitive to other environmental conditions as shown by a study on reaction centers of purple bacteria embedded in trehalose glasses (*20*). The temperature dependence of electron-transfer processes has already been correlated with the onset of protein flexibility of the reaction center protein (*11*, *21*−*23*).

So far, protein dynamics in PS II has only been investigated by Mössbauer spectroscopy using the non-heme iron ^{57}Fe in the close vicinity of the Q_A and Q_B sites as a probe for the averaged mean square displacement of the surrounding protein (*11*). However, protein dynamics can be directly observed using quasielastic neutron scattering (QENS) because of the high incoherent scattering cross section of hydrogen atoms and their almost homogeneous distribution in biomolecules. QENS has been widely used to study diffusive (see, e.g., refs *24*−*26*) as well as vibrational dynamics of proteins (*27*, *28*). QENS experiments revealed that proteins generally undergo a dynamical transition corresponding to the onset of localized diffusive protein motions at about 230 K in aqueous solution (*29*). Similar effects were observed for both native membrane-bound proteins (*24*) and lipid-bilayers as well as lipid−protein systems (*30*). As shown for lysozyme, however, the protein dynamics depends largely on the environment with water and glycerol acting as plasticizer and stabilizer, respectively (*31*). In general, the dynamical transition is suppressed upon dehydration and significantly affected by solvents of different viscosity, such as glycerol, sucrose, or trehalose (*32*−*37*). Likewise, the dynamics of hydration water molecules, that is, water molecules bound at the surface of proteins or lipid bilayers, is significantly slowed down (see, e.g., refs *24*, *38*, *39*) compared to that observed in bulk water (*40*). Among membrane proteins, bacteriorhodopsin (BR) is best characterized by QENS (see ref *24* and references therein) and can therefore serve as a prototype for investigations of the structure−function relationship at the atomic level. In this case, the thermal activation of localized diffusive atomic and molecular motions of the macromolecular protein−membrane complex could be correlated with its temperature-dependent functional activity as a proton pump (*41*).

In the present contribution, QENS studies were performed in order to elucidate the temperature and hydration dependence of protein dynamics in PS II membrane fragments. The comparison of the QENS data with results obtained by optical spectroscopy opens the pathway to unravel correlations between protein flexibility and the functional competence of PS II. The results of this study provide further support for a crucial role of protein flexibility for two effects of functional importance: (a) the thermally activated onset of electron transport from Q_A^- to Q_B (*11*) and (b) the blockage of Q_A^- reoxidation by Q_B at low hydration levels (*16*).

MATERIALS AND METHODS

Sample Preparation. PS II membrane fragments were obtained from spinach (*Spinacea oleracea*) following the procedure described by Berthold et al. (*42*) with modifications according to Völker et al. (*43*). All samples were washed three times in a buffer solution containing D_2O, 50 mM MES (pD 6.5), 0.4 M sucrose, 15 mM NaCl, and 10 mM $CaCl_2$. Finally, the sample material was divided into two sets with a dry weight of ∼300 mg each. The first set was equilibrated using the D_2O vapor of a relative humidity (r.h.) of 90%, whereas the second fraction was vacuum-dried. Two sets of buffer samples were prepared under identical conditions for separate QENS measurements.

The water content of the sample set hydrated at 90% r.h. was ∼45% of its dry mass. PS II membrane fragment samples were characterized by small angle scattering (SANS) using the membrane diffractometer V1 and the multidetector of V3 NEAT (BENSC, HMI Berlin, Germany).

Measurements of flash-induced oxygen evolution (*44*) revealed that D_2O-hydrated PS II membrane fragments remain functionally competent. Laser flash-induced absorption changes at 830 nm (*45*) and fluorescence quantum yield measurements (*46*) prove that both the reduction of $P680^{+\bullet}$ by Y_Z and the reoxidation of Q_A^- by Q_B remain fully active with retarded kinetics upon D_2O hydration.

QENS Measurements. Quasielastic neutron scattering (QENS) experiments were performed at the time-of-flight spectrometer NEAT (*47*, *48*) at BENSC (Hahn-Meitner Institute, Berlin, Germany). QENS spectra were measured with an incident neutron wavelength of 5.1 Å (∼3.2 meV) corresponding to an elastic Q range of 0.3−2.3 $Å^{-1}$. The elastic energy resolution determined by vanadium standard runs was $\Delta E = 0.093$ meV. QENS data were corrected for empty cell contribution, detector efficiency, and sample geometry dependent attenuation, normalized to the integrated vanadium intensity as well as converted to energy scale using the program package FITMO-4 (*49*). To ensure a proper correction of temperature-dependent QENS spectra, empty cell runs were recorded for five representative T values between 5 and 300 K and interpolated to yield spectra for intermediate temperatures. The sample transmission was approximately 96% so that multiple scattering artefacts should be negligible in the QENS data. For each separate measurement, the sample cell was placed carefully at the same position relative to the incident neutron beam in order to avoid normalization errors in buffer subtraction. Before subtraction, the buffer spectra were normalized by weight to determine their contribution to the total sample scattering.

The sample temperature was maintained using an Orange Cryofurnace and stabilized by a Lakeshore temperature controller. Prior to neutron scattering measurements, the temperature was allowed to equilibrate for 60 min.

Theoretical Background. In an incoherent QENS experiment, the measured quantity is the double-differential cross section (*50*, *51*), which describes the number of neutrons scattered into a solid angle element $\delta\Omega$ and an energy transfer element $\delta\omega$

$$\frac{\delta^2\sigma}{\delta\Omega\delta\omega} = \frac{|\mathbf{k}_1|}{|\mathbf{k}_0|}[b_{\mathrm{inc}}{}^2 S_{\mathrm{inc}}(\mathbf{Q}, \omega)] \quad (1)$$

where $\boldsymbol{k_0}$ and $\boldsymbol{k_1}$ are the wave vectors of incident and scattered neutrons, respectively, b_{inc} is the incoherent scattering length, $S_{\mathrm{inc}}(\mathbf{Q},\omega)$ is the incoherent scattering function with $\boldsymbol{Q}$ being the momentum transfer defined by $\boldsymbol{Q} = \boldsymbol{k_1} - \boldsymbol{k_0}$, and $\hbar\omega$ reflects the energy transfer (*52*). The function $S_{\mathrm{inc}}(\mathbf{Q},\omega)$ is related to the Van Hove self-correlation function $G_S(\mathbf{r},t)$ by the following equation (*50*, *51*):

$$S_{\mathrm{inc}}(\mathbf{Q}, \omega) = \frac{1}{2\pi}\int_{-\infty}^{\infty} e^{-i\omega t}\int_{-\infty}^{\infty} e^{i\mathbf{Q}\mathbf{r}}\, G(\mathbf{r}, t)\, \mathrm{d}\mathbf{r}\, \mathrm{d}t \quad (2)$$

where, in the classical approximation, $G_S(\mathbf{r},t)$ is the average time-dependent probability density distribution of the hydrogen atoms in the studied sample. In practice, $S_{\mathrm{inc}}(\mathbf{Q},\omega)$ needs to be replaced by an experimental scattering function $S_{\mathrm{exp}}(\mathbf{Q},\omega)$ with

$$S_{\mathrm{exp}}(\mathbf{Q},\omega) = \mathrm{F_N R}(\mathbf{Q},\omega) \times S_{\mathrm{theo}}(\mathbf{Q}, \omega) \quad (3)$$

which is composed of a normalization factor F_N and the convolution of an experimentally obtained resolution function $R(\mathbf{Q},\omega)$ with a theoretical model function $S_{\mathrm{theo}}(\mathbf{Q},\omega)$ describing the dynamics of the sample system. The neutron scattering spectra are compared to the following expression:

$$S_{\mathrm{theo}}(\mathbf{Q},\omega) = \mathrm{e}^{-\langle \mathrm{u}^2\rangle \mathrm{Q}^2}\left\{\mathrm{A}_0(\mathbf{Q})\delta(\omega) + \exp\left(-\frac{\hbar\omega}{2\mathrm{kT}}\right)\times \sum_n \mathrm{A}_n(\mathbf{Q})\mathrm{L}_n(\mathrm{H}_n, \omega) + S_{\mathrm{in}}(\mathbf{Q},\omega)\right\} \quad (4)$$

In this phenomenological description, the scattered intensity consists of three contributions, a $\delta(\omega)$-shaped elastic component, a sum of quasielastic Lorentzian-shaped components $L_n(H_n,\omega)$ with half-width at half-maximum (HWHM) H_n, and an inelastic part $S_{\mathrm{in}}(\mathbf{Q},\omega)$ describing low-frequency, moderately damped vibrational motions. Here $\exp[-\hbar\omega/2kT]$ is the detailed balance factor. The fractional intensities of the elastic and quasielastic contributions are given by the elastic and quasielastic incoherent structure factors (EISF and QISF), $A_0(Q)$ and $A_n(Q)$, respectively. The term $e^{-\langle u^2\rangle Q^2}$ is the Debye−Waller factor characterized by the global vibrational mean square displacement $\langle u^2\rangle$.

The quasielastic term stands for the correlation functions due to localized diffusive (i.e., confined stochastic) motions exhibiting a multiexponential decay in time, which are considered to be an important part of the internal motions of proteins or lipids. This type of decay is well known for specific situations, such as confined atomic or molecular diffusion, e.g., between a finite number of discrete sites, on a spherical surface (*53*), or in a spherical cavity (*54*), which lead to scattering functions comprising finite or infinite series of Lorentzian components $L_n(H_n,\omega)$, respectively. Another approach would consist in replacing the multiexponential decay model by a Kohlrausch−Williams−Watt (KWW) function (*55*) yielding a stretched exponential decay. Furthermore, the fractional Fokker−Planck equation (*56*) has been proposed recently for constructing non-exponentially decaying solutions (*26*), and last but not least, the model of coupled Langevin oscillators describing multiscale relaxation dynamics has been applied recently (*57*, *58*). Analogous methods of calculation could in principle be applied to the much more complex geometries encountered in biological systems like Photosystem II. Given the size of this system under study here and the related mathematical complexity, however, any of these approaches would certainly be beyond the scope of the present work. The second, equally relevant reason for refraining from such implied theoretical complexity is that the experiment being analyzed was carried out with a single value of the energy resolution. As a consequence, the observation time window is rather restricted and does not allow us to distinguish more than a very small number of different Lorentzian components, in the actual case only two. For the same reason, rather than aiming at a characterization of the sample dynamics on time scales extending over several orders of magnitude, we have to restrict the analysis to the available observation time window and intend to obtain information on the dynamical behavior within this window, for different levels of hydration and as a function of temperature. For this purpose, two phenomenological Lorentzian components employed appear to be sufficient.

For the inelastic scattering function $S_{\mathrm{in}}(\mathbf{Q},\omega)$, a damped harmonic oscillator (DHO) scattering function derived in the framework of linear response theory and using the fluctuation−dissipation theorem (see for instance ref *59*) is employed as a realistic model. The well-known frequency distribution of this model has been applied for describing inelastic low-energy spectral features in many different areas in the past. Examples of very different types include superfluid ^{4}He (*60*), heavy water at room temperature (*61*), hydration water in porcine stratum corneum (*39*), and the purple membrane of *Halobacterium salinarum*. In the latter case, in order to meet the requirements of the sum rules and the correct dimensionality, the DHO frequency distribution has been included with proper normalization into the total incoherent scattering function, as follows (*62*):

$$S_{\mathrm{in}}(\mathbf{Q},\omega) = (\mathrm{e}^{\langle \mathrm{u}^2\rangle_{\mathrm{DHO}}\mathrm{Q}^2} - 1)\frac{\omega}{\pi\mathrm{kT}(\mathrm{e}^{\hbar\omega/\mathrm{kT}} - 1)}\frac{\Gamma \mathrm{E}^2}{(\mathrm{E}^2 - \omega^2)^2 + \omega^2\Gamma^2} \quad (5)$$

Here, $\langle u^2\rangle_{\mathrm{DHO}}$ is the mean square displacement of the DHO, E the DHO frequency, and Γ the DHO damping. It should be noted that we are employing eq 5 as a purely phenomenological model. Although it explicitly contains only one single DHO frequency E, an appropriate choice of the damping factor Γ provides a broad and relatively flat

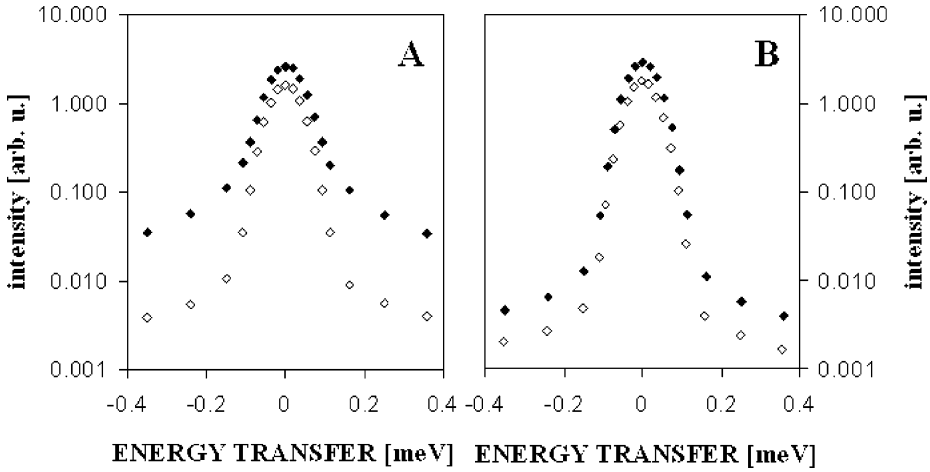

FIGURE 1: Comparison of QENS spectra of PS II membrane fragments (♦) and the corresponding buffer solution (◇) for two different hydration levels, i.e., 90% r.h. (frame A) and vacuum-dry (frame B), respectively. The spectra were obtained with an incident neutron wavelength of 5.1 Å and an elastic resolution of 0.093 meV at a scattering angle of 75.3° and at a temperature of 300 K.

frequency distribution, which describes the vibrational part of the observed neutron spectra very well and permits the separation of the latter from the quasielastic components, which are due to confined stochastic motions mainly of small side groups in biological macromolecules represented by eq 4.

Considering only the elastic contribution to eq 5, one can define a temperature-dependent total mean square displacement $\langle u^2\rangle_{total}$ by the following equation:

$$\langle u^2\rangle_{total}(T) = \langle u^2\rangle - \frac{1}{Q^2}\ln A_0(Q) = -\frac{1}{Q^2}\ln S_{elast}(T) \qquad (6)$$

The term $\langle u^2\rangle_{total}$ is identical to the vibrational mean square displacement $\langle u^2\rangle$ when quasielastic scattering is absent at low temperatures, that is, the EISF A_0 is equal to one. Otherwise, diffusive localized motions contribute via the term $\ln A_0(Q)$, which becomes constant in the so-called Gaussian approximation at very low Q.

RESULTS

QENS spectra were measured at temperatures between 5 and 300 K for both the dry and the hydrated sample as well as buffer solutions prepared under identical conditions. The buffer composition is given in detail in the Materials and Methods section. Typical spectra of hydrated PS II membrane fragments and the corresponding buffer solution obtained at 300 K are compared in frame A of Figure 1. An inspection of these data reveals that the main contribution to the quasielastic region originates from PS II membrane fragments (note the logarithmic scaling). Especially below 240 K, the QENS spectra of the buffer solution are widely dominated by elastic scattering consistent with a crystalline character (not shown). QENS spectra of the dry sample and the corresponding buffer solution measured at 300 K are compared in frame B of Figure 1. Here, the quasielastic contribution to both spectra is significantly suppressed compared to those shown in frame A of Figure 1. Nevertheless, the quasielastic broadening present in the spectrum of dry PS II membrane fragments is more pronounced than in the corresponding buffer solution. For further analysis, the buffer contribution was subtracted from the QENS spectra of PS II membrane fragments.

Typical QENS spectra obtained for PS II membrane fragments hydrated at 90% r.h. are shown in Figure 2 for three representative temperature values of 100, 200, and 300 K. The QENS spectra obtained at 100 and 200 K appear to be dominated by elastic scattering. In comparison to the representation chosen in Figure 1, the double logarithmic plot reveals that the elastic peak is accompanied by a well-separated Boson peak. The spectra differ mainly in a very weak quasielastic contribution visible at 200 K (indicated by an arrow in Figure 2). The latter component is completely absent at 100 K. At 300 K, a strong quasielastic contribution appears, which clearly overlaps the inelastic contribution.

To investigate the influence of hydration on protein dynamics in PS II membrane fragments, QENS spectra were also measured for a vacuum-dried sample in the same temperature range, that is, between 5 and 300 K. Typical QENS spectra obtained for dry PS II membrane fragments are shown in Figure 3 for temperature values of 100, 200, and 300 K. As for the hydrated sample, the QENS spectrum obtained at 100 K exhibits predominantly elastic scattering. A quasielastic contribution becomes visible at 200 and 300 K. However, at 300 K, the latter contribution is significantly smaller than that in hydrated PS II (cf. Figure 2).

A more detailed analysis of the QENS spectra of hydrated and dry PS II membrane fragments is achieved by employing phenomenologic fits according to eq 4. In order to minimize the number of free parameters in each fit, an iterative three-step fit procedure has been used. First, the data at all temperatures were fit using a single quasielastic component with a Lorentzian width (HWHM) of 0.1135 meV and a flat background. The elastic intensity approximated by these fits was used to calculate $\langle u^2\rangle_{total}$ according to eq 6 (Figure 4). Below 120 K, there is a linear increase of $\langle u^2\rangle_{total}$ for both the hydrated and the dry sample, which is typical for harmonic vibrational motions (see range A in Figure 4), that is, $\langle u^2\rangle_{total}$ should mainly reflect the vibrational mean square displacement $\langle u^2\rangle_{vib}$. An extrapolation to higher temperatures of this anticipated linear function for $\langle u^2\rangle_{vib}$ is given by the solid line in Figure 4. Consequently, these values are used as an upper limit for the vibrational mean square displacement at each temperature in the further analysis.

In a second step, a damped harmonic oscillator (DHO) function described by eq 5 is added as a realistic inelastic

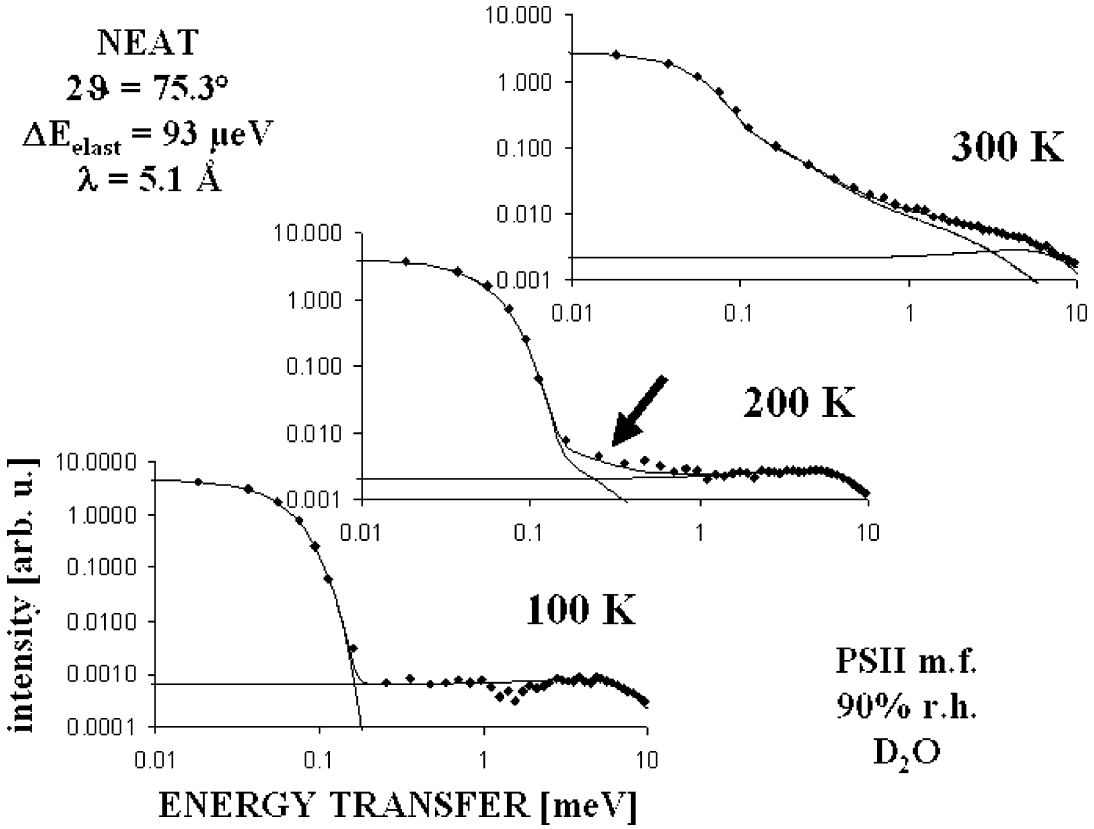

FIGURE 2: Double-logarithmic plots of QENS spectra of PS II membrane fragments hydrated in D_2O vapor of 90% r.h. (♦) obtained with an incident neutron wavelength of 5.1 Å and an elastic resolution of 0.093 meV, at a scattering angle of 75.3° and temperatures of 100, 200, and 300 K. The black solid line is a phenomenological fit of the data, and the gray lines correspond to the quasi and inelastic contributions to the fit. The weak quasielastic contribution emerging at 200 K is indicated by an arrow. Note the different scaling of the spectra obtained at 100 K.

contribution to eq 4. The resulting model function is fit to the low-temperature spectra, where quasielastic broadening is absent (range A in Figure 4) to determine the line shape of the DHO term (see solid line in the lower spectrum of Figure 2). The DHO function derived from this fit has an energy ω of 8.50 meV and a damping Γ of 10 meV for hydrated PS II membrane fragments. In the case of dry PS II membrane fragments, the DHO energy ω shifts to 7.65 meV, while the damping Γ remains at 10 meV. Both sets of parameters lie in the typical range for low-frequency protein vibrations. Thus, the line shape appears to be well suited to describe the inelastic part of the QENS spectra in the low-temperature range investigated in this study. The $\langle u^2\rangle_{DHO}$ values derived from the fits, however, are a factor of 2 smaller than $\langle u^2\rangle_{vib}$ at each T value for both the hydrated and the dry sample, that is, the DHO accounts for only half of the total vibrational intensity.

Finally, the QENS spectra of hydrated and dry PS II membrane fragments obtained at higher temperatures (ranges B and C in Figure 4) are fit according to eq 4. Some representative fits are shown in Figures 2 and 3. A number of the parameters used have been determined separately above and are fixed accordingly, that is, the line shape of the DHO function and the vibrational mean square displacement $\langle u^2\rangle_{vib}$. In the case of the DHO term, thermal population is taken into account according to Bose−Einstein statistics (see eq 5). The vibrational mean square displacement for each temperature is calculated by linear extrapolation of $\langle u^2\rangle_{total}$ to higher temperatures (see solid line in Figure 4), while the DHO mean square displacement $\langle u^2\rangle_{DHO}$ is treated as a free parameter. This approach leads to a well-defined line shape of the DHO in the quasielastic region, which differs from that of a flat background. Thus, it also affects the fit of the quasielastic components. A good overall description of the QENS spectra shown in Figures 2 and 3 requires a minimum of two Lorentzian components at 300 K, a component with a width (HWHM) of 0.1135 meV corresponding to a slow relaxation time of 5.8 ps, and another one having a width (HWHM) of 2.467 meV corresponding to a faster relaxation time of 0.3 ps. When using this phenomenological approach, one has to keep in mind that the above two relaxation times reported here do actually represent a broad spectrum of relaxation rates (see, e.g., ref *26* for a detailed discussion). The slow component is also present at 200 K as indicated by the arrow in Figure 2. The Lorentzian widths were kept constant at all temperature values, while the corresponding structure factors, hereafter referred to as $QISF_1$ and $QISF_2$ for the slow and fast component, respectively, were treated as free parameters.

Fits of quality similar to those shown in Figures 2 and 3 have been obtained for all QENS spectra in the temperature range between 5 and 300 K. As described above, elastic intensities from these fits were used to determine the total average mean square displacement $\langle u^2\rangle_{total}$ in the whole temperature range under study according to eq 6. The temperature dependence of $\langle u^2\rangle_{total}$ shown in Figure 4 reveals three characteristic T ranges. In range A, below 120 K there is a linear increase in $\langle u^2\rangle_{total}$, which is typical for harmonic vibrational motions (see above). Deviations from the linear behavior of the total mean square displacement are visible

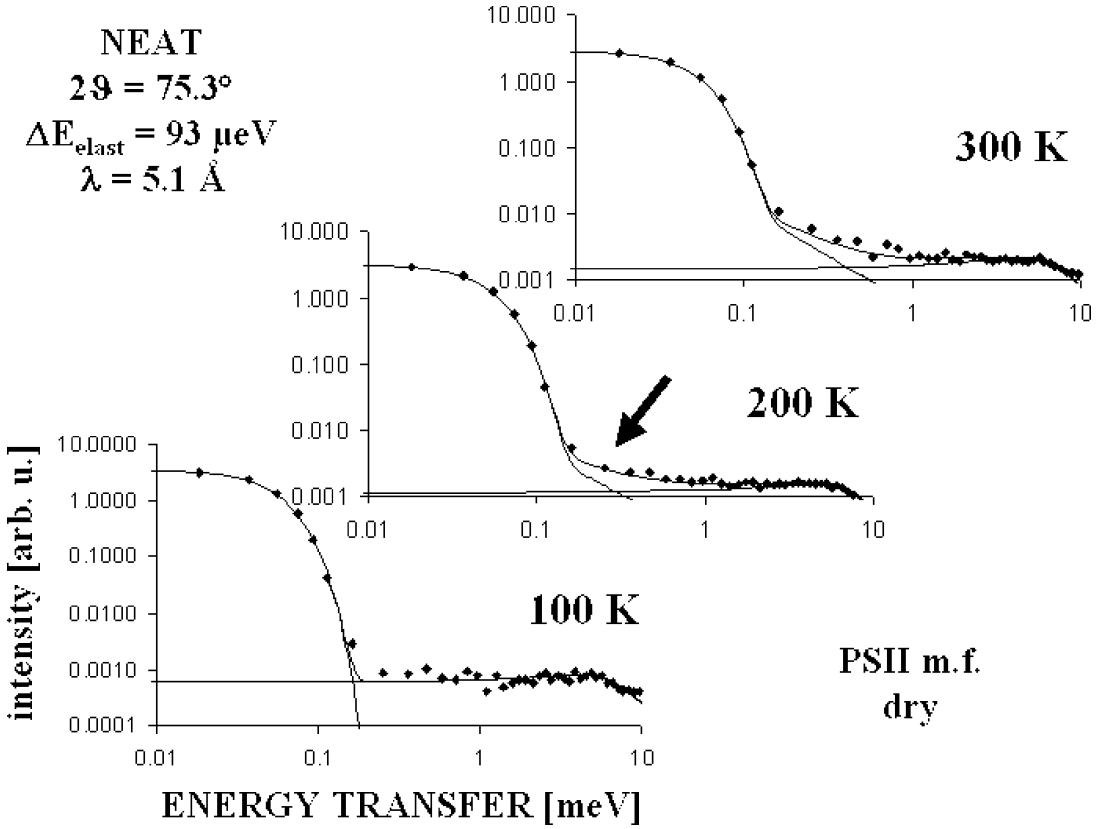

FIGURE 3: Double-logarithmic plots of QENS spectra of vacuum-dried PS II membrane fragments (♦) obtained with an incident neutron wavelength of 5.1 Å and an elastic resolution of 0.093 meV, at a scattering angle of 75.3° and temperatures of 100, 200, and 300 K. The black solid line is a phenomenological fit of the data, and the gray lines correspond to the quasi and inelastic contributions to the fit. The weak quasielastic contribution emerging at 200 K is indicated by an arrow. Note the different scaling of the spectra obtained at 100 K.

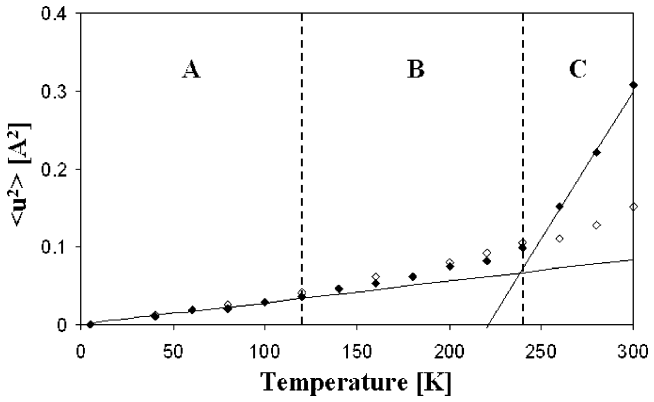

FIGURE 4: Temperature dependence of the average atomic mean square displacement $\langle u^2 \rangle_{total}$ obtained from the elastic intensity of QENS spectra for hydrated (♦) and dry PS II (◊). The solid lines are given for ease of inspection. The three temperature ranges discussed in the text are labeled by indices A, B, and C.

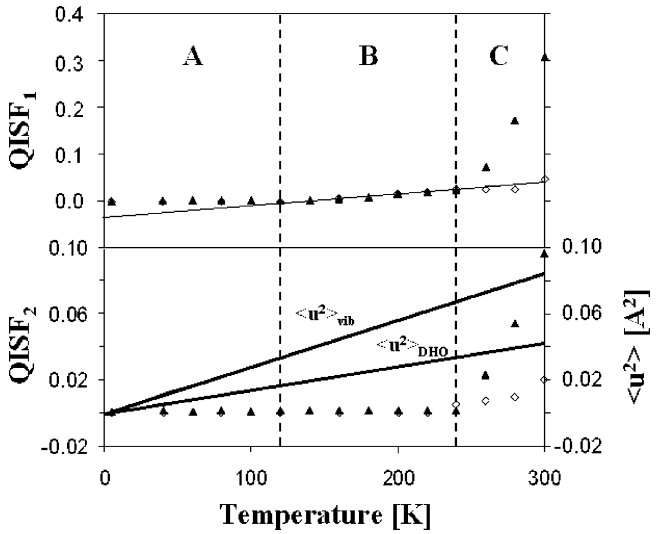

FIGURE 5: Temperature dependence of $QISF_1$ and $QISF_2$ for hydrated (▲) and dry (◊) PS II membrane fragments as obtained from the phenomenological fits shown in Figures 2 and 3. Note the different scaling in the two frames. The thin solid line is meant to guide the eye. The thick solid lines in the lower frame give the $\langle u^2 \rangle_{vib}$ (upper line) and $\langle u^2 \rangle_{DHO}$ values (lower line) used in the fits shown in Figures 2 and 3 (see right scale).

above 120 K (range B) and above 240 K (range C) for hydrated PS II membrane fragments. Surprisingly, a small deviation from the linear behavior of the total mean square displacement above 120 K (range B) is also visible for the dry sample. However, the transition observed at 240 K (range C) is by far less apparent than that in hydrated PS II. Thus, the main difference in dynamical behavior caused by hydration is seen in the presence (or absence) of the dynamical transition at 240 K.

The temperature dependence of the QISFs of the two Lorentzian components obtained for hydrated PS II membrane fragments is shown in Figure 5. The $\langle u^2 \rangle_{DHO}$ values of the hydrated sample appear to be a factor of 2 smaller than $\langle u^2 \rangle_{vib}$ at each T value (see lower frame in Figure 5). Both QISFs exhibit a quite similar temperature dependence with a significant increase starting at 240 K. Since this effect is co-incident with the main transition observed for $\langle u^2 \rangle_{total}$, it can be concluded that the deviation from the linear temper-

ature dependence of $\langle u^2 \rangle_{total}$ above 240 K is due to the thermal activation of anharmonic, diffusive protein motions at about 240 K with mean relaxation times of 5.8 and 0.3 ps, respectively (region C). A closer inspection of $QISF_1$ corresponding to the slow Lorentzian component reveals a second transition at about 120 K (see upper frame in Figure 5). This transition is co-incident with the (slight) deviation from the linear temperature dependence of $\langle u^2 \rangle_{total}$ observed at 120 K (Figure 4) and corresponds to the weak quasielastic contribution present at 200 K (Figure 2). This indicates that there is also a thermal activation of diffusive protein motions with a mean relaxation time of 5.8 ps at temperatures as low as 120 K (region B).

The temperature dependence of the QISFs obtained for dry PS II membrane fragments is also shown in Figure 5. The $\langle u^2 \rangle_{DHO}$ values are similar to those of the hydrated sample, and thus are a factor of 2 smaller than $\langle u^2 \rangle_{vib}$ at each *T* value. An inspection of Figure 5 reveals that there is an onset of diffusive protein motions at 120 K similar to that observed in the hydrated sample. The strong increase of both QISFs observed for the hydrated sample above 240 K, however, is not present in the dry sample. Thus, the strong suppression of protein mobility visible in the temperature dependence of $\langle u^2 \rangle_{total}$ of dry PS II membrane fragments (Figure 4) is also reflected in the small values determined for the QISFs of the two Lorentzian components.

In summary, the dynamics of PS II membrane fragments hydrated at 90% r.h. is characterized by purely harmonic vibrational motions at temperatures lower than 120 K, which is indicated by the absence of quasielastic scattering and a linear increase in $\langle u^2 \rangle_{total}$ with increasing temperature. The temperature dependence of both the QISFs of the two Lorentzian fit components and of $\langle u^2 \rangle_{total}$ in ranges B and C suggests the onset of diffusive protein motions due to the availability of additional conformational substates at 120 and 240 K, respectively. The dynamics of hydrated and dry PS II membrane fragments is virtually similar at low temperatures (<240 K), while a striking difference emerges at temperatures above 240 K due to the strong suppression of diffusive protein motions in the dry sample, that is, protein flexibility is significantly reduced at physiological temperatures.

DISCUSSION

The sample type used in the present study was characterized by electron microscopy and biochemical methods and found to consist of oxygen-evolving membrane fragments from the grana stacks of plant thylakoids (*63*). These preparations are highly enriched in functionally competent Photosystem II complexes and form widely flat stacks of two membrane fragments, which are lacking the round-shaped edges typical for thylakoids. Neighboring membranes appeared to be associated at the acceptor side of the PS II complexes. The polypeptide composition of PS II is quite complex, comprising at least 20 polypeptides (*64*). The PS II core consisting of the D1/D2 heterodimer and associated cofactors, CP47, CP43, Cytb 559, and smaller subunits, is surrounded by the minor and major Chl a/b-containing light-harvesting complexes (*65*). It adds to the complexity of the system that lipid molecules not only form the membrane bilayer but also appear as intrinsic constituents of PS II (*7*). Therefore, the dynamics observed in this study should be regarded as that of a protein−lipid system.

Despite the complex composition of the sample system, the temperature dependence of the QISFs (Figure 5) and the average atomic mean square displacement $\langle u^2 \rangle_{total}$ of hydrated PS II membrane fragments (Figure 4) revealed three different temperature regions that can be clearly distinguished by the active type(s) of protein dynamics. The deviation of $\langle u^2 \rangle_{total}$ from linearity in regions B and C is due to the appearance of quasielastic scattering in the QENS spectra (Figure 5). The presence of two transition temperatures at about 120 and 240 K is qualitatively similar to results reported for bacteriorhodopsin (see, e.g., refs *24*, *66*). This striking similarity suggests that the two distinct transition temperatures and the corresponding types of thermally activated protein motions could be a general feature of membrane proteins. In the case of bacteriorhodopsin, the protein dynamics on the ps-time scale has mainly been attributed to localized diffusive motions within the protein−membrane complex encompassing three different types of motions: (a) fast methyl group reorientation, (b) jump diffusion of protons located in hydrogen bonds, and (c) slower reorientational motions of larger protein residues (*67*). Molecular dynamics simulations of C-Phycocyanin assigned the main anharmonic contribution to the incoherent scattering function to motions of side chains relative to the protein backbone (*57*).

The main transition temperature of 240 K obtained for the PS II membrane fragments (Figure 2) is quite similar to the results of Mössbauer spectroscopy (*11*). The transition at 120 K, however, seems to be absent in this data set. It has to be noted at this point that QENS is mainly sensitive to protons that are almost evenly distributed in proteins and lipids, whereas the Mössbauer experiments use the non-heme iron ^{57}Fe located between the Q_A and Q_B sites as a probe for the protein dynamics. Thus, a comparison of the complementary results from Mössbauer spectroscopy and QENS can lead to identification of the protein motions characteristic for the overall multimeric protein complex and those relevant to the vicinity of the Q_A and Q_B sites, which are involved in the functionally important charge-transfer processes in the PS II RC. The nature of the protein motions in the three identified temperature ranges A−C and their functional relevance will be discussed in the following paragraphs.

Vibrational Dynamics at Low Temperatures (Range A). The linear increase in $\langle u^2 \rangle_{total}$ with increasing temperature (Figure 4) in range A (T < 120 K) originates from purely harmonic vibrational motions. Thus, the QENS spectra of hydrated and dry PS II membrane fragments are composed of elastic and inelastic contributions only (Figures 2 and 3). The inelastic part resembles the well-known Boson peak, which is characteristic for disordered systems such as proteins and lipids. Similar low-temperature dynamical behavior has recently been reported for the solubilized trimeric antenna complex LHC II (*68*), which is a constituent of PS II supercomplexes (*65*).

In hydrated PS II membrane fragments, the inelastic part can be modeled, within the considered energy transfer range, using a damped harmonic oscillator function (DHO) with an energy of 8.5 meV and a damping of 10 meV. Thus, the DHO reflects the broad distribution of low-frequency protein vibrations (phonons) of PS II. The mean square displacement of the DHO, however, was found to be a factor of 2 lower

than $\langle u^2 \rangle_{total}$, that is, the DHO accounts for only about 50% of full vibrational intensity. This is quite plausible given the limited energy transfer range of up to 10 meV (80 cm^{-1}). This window is exceeded, for example, by the localized vibrations of the pigments bound in the RC and antennae of PS II, which fall into the 40−220 meV (320−1760 cm^{-1}) range (*69*). Note, however, that a quantitative comparison of vibrational intensities in optical and neutron scattering spectra is precluded by the possible presence of frequency-dependent coupling strengths and selection rules for particular vibrational frequencies in optical spectra (see, e.g., ref *68* and references therein). Regardless of this fact, it is interesting that in ref *69*, the integral Huang−Rhys factors reflecting the electron vibrational coupling strengths *S* for protein and chlorophyll vibrations in the antenna complex LHC II were found to be quite similar at 0.8 and 0.43, respectively. This supports our finding that the low-frequency protein vibrations reflected by the DHO term constitute only about 50% of the total vibrational contribution to the QENS spectra of PS II membrane fragments.

In dry PS II, the DHO energy is shifted to 7.65 meV, that is, to a smaller value than that observed for the hydrated sample. Thus, there seems to be a shift of the protein vibrations toward smaller frequencies with decreasing hydration level. Similar observations have already been reported for other proteins such as myoglobin (*70*), β-lactoglobulin (*71*), and pig liver esterase (*72*) as well as those from computer simulations (*73*). This effect would be consistent with a strengthening of the force constants of the protein system with increasing hydration. Accordingly, it was suggested that the increased rigidity is due to hydrogen bond formation between hydration water molecules and solvent-exposed external protein residues (*74*). More recently, inelastic neutron scattering of partially deuterated β-lactoglobulin (*71*) revealed that external residues display lower vibrational frequencies than the protein backbone in the dry protein. It was concluded that surface residues are involved in more delocalized, intermolecular, vibrations than the protein core in the dehydrated state. In contrast, in the hydrated protein, external and internal protein regions displayed similar vibrational frequencies so that the corresponding vibrations should be restricted to similar localization domains. Low-frequency inter-protein vibrations have also been reported from recent molecular dynamics simulations of myoglobin (*75*). Thus, the shift of the DHO energy with dehydration of PS II membrane fragments appears to be in line with QENS and simulation results obtained for other protein systems.

Protein Dynamics at Intermediate Temperatures (Range B). In the intermediate temperature range of 120 K < *T* < 240 K (range B), the protein dynamics of dry and hydrated PS II membrane fragments is characterized by a predominantly linear temperature dependence of $\langle u^2 \rangle_{total}$ and small values of the QISFs corresponding to the two quasielastic contributions to the QENS spectra. This indicates that the protein dynamics observed is quite similar to that described for the low-*T* range A with mainly harmonic vibrational motions.

However, there is a small deviation from the linear increase of $\langle u^2 \rangle_{total}$ with increasing temperature starting at about 120 K (Figure 4). This effect is mirrored by a small increase in $QISF_1$ corresponding to the narrow quasielastic contribution (see upper frame of Figure 5). Thus, there is an onset of protein mobility at 120 K, which is observed almost similarly in both dry and hydrated PS II membrane fragments. Accordingly, this transition is not related to the hydration state of the protein. The presence of some protein flexibility at temperatures below the dynamical transition has also been reported for other proteins (*72*, *76*) and is consistent with recent simulations of methyl group dynamics in RNase (*77*). The results in refs *76* and *77* suggest that the onset of methyl group rotations could be responsible for the slightly non-harmonic behavior of $\langle u^2 \rangle_{total}$ above 120 K.

Interestingly, the transition at 120 K was absent in the Mössbauer data of PS II membrane fragments using the non-heme iron ^{57}Fe as a probe for protein flexibility (*11*). This means that the dynamical processes responsible for the increase in $\langle u^2 \rangle_{total}$ may not be present in the whole protein but should be more or less confined. It follows that depending on the degree of spatial localization, the actual amplitude of the respective protein motions can be larger than indicated by the small increase in $\langle u^2 \rangle_{total}$ because QENS gives an average measure for the mobility of all hydrogen atoms in the studied pigment−protein−lipid system.

Observation of an onset of protein mobility at 120 K is most interesting since it correlates with changes observed in the fluorescence properties of the PS II (and other)−antenna complexes. For instance, a remarkable red-shift of the fluorescence spectrum of LHC II occurs above 120 K (*78*), which is inconsistent with the low-energy Q_y level structure assigned by hole-burning experiments at 4.2 K (*79*). A similar effect has been reported for the absorption bands of individual Chl molecules of LHC II as determined using reconstituted LHC II lacking individual Chls (*80*). A shift emerging at about 150 K has also been observed for the B850 band of bacterial LH2 (*81*). So far, an interpretation for these effects was given in terms of crystal expansion, that is, larger atomic displacements due to an increasing anharmonicity of the protein vibrations lead to an increasing Stokes shift with increasing temperature. On the basis of the results of the present study, however, the thermal activation of diffusive protein motions at about 120 K appears to be responsible for the observed changes in the fluorescence properties of the LHC II−antenna complex. This is plausible, if these protein motions represent or accompany conformational changes between thermally activated protein substates in the vicinity of pigments. Such conformational changes may affect the potential experienced by the chromophore and induce significant shifts in their site energies (*82*), which are also visible in hole burning (*83*) and single-molecule spectroscopy (*84*).

Protein Dynamics at Higher Temperatures (Range C). The most pronounced change in the temperature dependence of the QISFs and of the total mean square displacement $\langle u^2 \rangle_{total}$ is observed for hydrated PS II membrane fragments at about 240 K. This finding indicates that at temperatures above 240 K (region C), a new thermally activated type of protein dynamics becomes effective. A comparison of the latter effect with the temperature dependence of the QISFs for the two fitted quasielastic components proves that the change in protein flexibility at about 240 K is due to the onset of diffusive (large-amplitude) protein motions (Figure 5). The similarity of the temperature dependence for the two Lorentzian components characterized by different time scales of

motion indicates a general effect on protein flexibility emerging at 240 K. This feature is characteristic for the so-called dynamical transition that has been observed for a number of proteins (*24*, *29*, *30*).

The dynamical transition at 240 K is clearly absent in dry PS II membrane fragments as reflected in both the temperature dependence of the total mean square displacement and the significantly smaller quasielastic contributions in the QENS spectra at room temperature. The latter finding is the most striking difference observed between dry and hydrated samples in this study. This implies that dehydration of PS II membrane fragments leads to a considerable freezing of protein flexibility, that is, dehydration has an analogous effect on protein dynamics as temperature decrease. Since protein mobility is activated in hydrated PS II membrane fragments, the dynamical transition observed at 240 K can be regarded as solvent-dependent, that is, water acts as a plasticizer for the protein−lipid system (*31*). In this sense, the dynamical transition at 240 K is essentially different from that at about 120 K, though both phenomena seem to originate from activation of diffusive protein motions. An analogous hydration dependence of the dynamical transition has been observed, for instance, for bacteriorhodopsin (*24*).

In addition to the presence of water, sucrose was used as a cryoprotectant in sample preparation (see the Materials and Methods section). As pointed out in the Introduction section, it is generally known that solvents of different viscosity affect both transition temperature and extent of protein flexibility above the dynamical transition. This was investigated in detail, for example, for lysozyme in ref *36*. In the present study, however, all experiments were performed at a constant sucrose concentration so that the temperature and hydration-dependent effects observed here are virtually free from artefacts due to a variation of sucrose concentration. However, the sucrose concentration has to be taken into account when comparing the results presented here to those of other studies. Therefore, it is important to note that the sucrose concentration of 0.4 M is identical to that used by Garbers et al. (*11*) and Kaminskaya et al. (*16*) when investigating the temperature and hydration dependence of Q_A^- reoxidation by Q_B in PS II membrane fragments.

In summary, the protein dynamics of PS II membrane fragments exhibits dependences on temperature and hydration, which are quite typical for protein systems. The intriguing phenomenon, however, is that the activation of protein dynamics appears to be the prerequisite for some important functional properties of PS II. This is illustrated in Figure 6, where the temperature dependence of the QISFs for hydrated PS II membrane fragments is compared to the efficiency of Q_A^- reoxidation by Q_B. The latter quantity was determined from the relaxation amplitude of the flash-induced normalized fluorescence quantum yield as a function of temperature (*11*, *12*). The similar temperature dependence suggests that there is an intimate correlation between the thermally activated onset of the electron transport from Q_A^- to Q_B and protein flexibility as monitored by QENS. The temperature dependence of $\langle u^2 \rangle$ for $T > 240$ K obtained by QENS for the overall protein−lipid system is strikingly similar to that gathered from Mössbauer spectroscopy for the protein environment of the non-heme iron ^{57}Fe, which is located between the binding sites of Q_A and Q_B (*7*). This coincidence indicates that the observed onset of protein

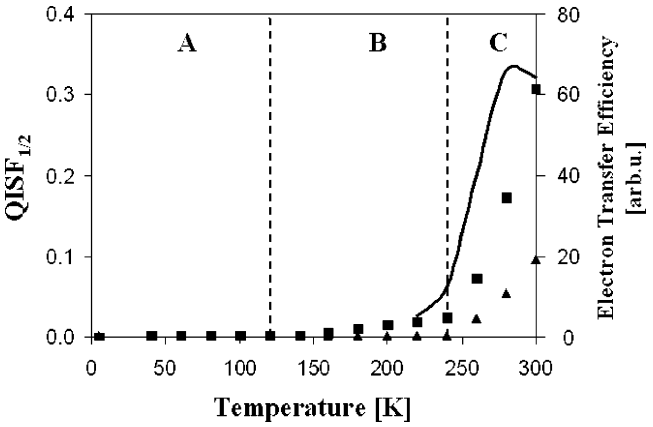

FIGURE 6: Temperature dependence of $QISF_1$ (■) and $QISF_2$ (▲) for hydrated PS II membrane fragments as obtained from the phenomenological fits shown in Figure 2. The increase of electron-transfer efficiency taken from ref *11* (solid line) with increasing temperature strictly correlating with the onset of protein flexibility in temperature region C.

mobility is also relevant for the protein domain in the vicinity of the Q_A and Q_B binding sites. In agreement with this conclusion, a number of studies provided evidence that the plasticizing effect of water extends across the whole protein rather than affecting only the external surface (*71*, *77*, *85*). Analogously, the freezing of protein mobility by dehydration is represented by the drastically smaller increase of both QISFs with increasing temperature in dry PS II (Figure 5). This effect appears to be responsible for the blockage of Q_A^- reoxidation by Q_B at hydration values lower than 45% r.h. reported by Kaminskaya et al. (*16*).

A similar correlation between protein flexibility and the efficiency of electron transport from Q_A^- to Q_B was found in the reaction center in chromatophores of purple bacteria (*22*). On the basis of X-ray crystallography, a drastic reorientation of the quinone headgroup of Q_B was inferred to be required for the formation of the semiquinone state Q_B^- in isolated reaction centers of *Rb. sphaeroides* (*86*). However, the idea of a simple conformational gating mechanism has been questioned (*87*) and is not supported by recent FTIR measurements (*88*, *89*) and a time-resolved X-ray crystallography study (*90*). In addition, it seems likely that the conformational changes required for Q_B reduction by Q_A^- comprise the rearrangement of hydrogen bonds, most prominently the reorientation of the Ser223 of the L-subunit (*91*, *92*). As discussed above, this is the type of motion probed by QENS on the ps-time scale (*67*). Thus, an analogous type of conformational triggering can be assumed to take place on the acceptor side of PS II. The assumption of a conformational change is also in line with the finding that Q_A^- reoxidation remains possible at much lower temperatures than 240 K, provided that the semiquinone state Q_B^- is populated by preillumination before freezing (*12*). It should be added that a functional role of protein mobility is also observed for distinct redox steps of the water oxidation leading to O_2 evolution in the WOC. This conclusion is strongly supported by the strikingly similar freezing temperatures of the $S_2 \rightarrow S_3$ and $S_3 \rightarrow\!\!\rightarrow S_0 + O_2$ reactions (*13*, *14*). Likewise, these redox transitions are also inhibited upon the dehydration of PS II core complexes from the thermophilic cyanobacterium *T. elongatus* (*17*). These findings emphasize the key role of protein flexibility for the reactions

of oxidative water cleavage and plastoquinol formation that are energetically driven by the radical ion pair $P680^+$ Q_A^- generated via light-induced charge separation in PS II.

CONCLUDING REMARKS

In the present study, quasielastic neutron scattering (QENS) experiments have been employed to study the protein dynamics in dry and hydrated PS II membrane fragments at temperatures between 5 and 300 K. For temperatures below 120 K, the protein dynamics of both dry and hydrated PS II is characterized by harmonic vibrational motions. The inelastic contribution resembles the well-known Boson peak, which is characteristic for disordered systems such as proteins and lipids. Two transitions visible in the temperature dependence of the total mean square displacement $\langle u^2 \rangle_{total}$ at 120 and 240 K can be correlated with the onset of localized diffusive protein motions with characteristic times of 5.8 and 0.3 ps in both dry and hydrated PS II membrane fragments. While the transition at 120 K appears to be virtually independent of the hydration degree, the dynamical transition at 240 K is clearly solvent-dependent because it is strongly suppressed in dry PS II membrane fragments.

The thermally activated onset of protein flexibility as monitored by QENS in hydrated PS II membrane fragments is shown to be correlated to the temperature dependence of the electron transport from Q_A^- to Q_B (*11*). Analogously, the freezing of protein mobility by dehydration in dry PS II membrane fragments appears to be responsible for the blockage of Q_A^- reoxidation by Q_B as observed for hydration values lower than 45% r.h (*16*). These findings emphasize the crucial functional relevance of protein flexibility for the reactions of oxidative water cleavage and plastoquinol formation in PS II of green plants.

ACKNOWLEDGMENT

We are also grateful to S. Kussin and M. Wess (TU Berlin) for their help in sample preparation as well as to G. Steiner and B. Urban (HMI Berlin) for technical assistance during the neutron scattering experiments.

REFERENCES

1. Ke, B. (2001) *Photosynthesis: Photobiochemistry and Photobiophysics*, Kluwer Academic Publishers, Dordrecht, The Netherlands.
2. Renger, G., and Holzwarth, A.R. (2005) Primary Electron Transfer, in *Photosystem II: The Water/Plastoquinone Oxido-Reductase in Photosynthesis* (Wydrzynski, T., and Satoh, K., Eds.) pp 139−175, Kluwer Academic Publishers, Dordrecht, The Netherlands.
3. Bernarding, J., Eckert, H.-J., Eichler, H.-J., Napiwotzki, A., and Renger, G. (1994) Kinetic studies on the stabilization of the primary radical pair $P680^+Pheo^-$ in different photosystem II preparations from higher plants, *Photochem. Photobiol. 59*, 566−573.
4. Petrouleas, V., and Crofts, A.R. (2005) The Iron−Quinone Acceptor Complex, in *Photosystem II: The Water/Plastoquinone Oxido-Reductase in Photosynthesis* (Wydrzynski, T., and Satoh, K., Eds.) pp 177−206, Kluwer Academic Publishers, Dordrecht, The Netherlands.
5. Kok, B., Forbush, B., and Mc Gloin, M. (1970) Cooperation of charges in photosynthetic O_2 evolution. I. A linear four step mechanism, *Photochem. Photobiol. 11*, 457−476.
6. Ferreira, K., Iverson, T. M., Maghlouni, K., Barber, J., and Iwata, S. (2004) Architecture of the photosynthetic oxygen-evolving center. *Science 303*, 1831−1838.
7. Loll, B., Kern, J., Sänger, W., Zouni, A., and Biesiadka, J. (2005) Towards complete cofactor arrangement in the 3.0 Å resolution structure of photosystem II, *Nature 438*, 1040−1044.
8. Hughes, J. L., Smith, P., Pace, R., and Krausz, E. (2006) Charge separation in photosystem II core complexes induced by 690−730 nm excitation at 1.7 K, *Biochim. Biophys. Acta 1757*, 841−851.
9. Joliot, P., and Joliot, A. (1973) Different types of quenching involved in Photosystem II centers, *Biochim. Biophys. Acta 305*, 302−316.
10. Renger, G. (1993) Water cleavage by solar radiation: an inspiring challenge of photosynthesis research, *Photosynth. Res. 38*, 229−247.
11. Garbers, A., Kurreck, J., Reifarth, F., Renger, G., and Parak, F. (1998) Correlation between protein flexibility and electron transfer from $Q_A^{-\bullet}$ to Q_B in PS II membrane fragments from spinach, *Biochemistry 37*, 11399−11404.
12. Reifarth, F., and Renger, G. (1998) Indirect evidence for structural changes coupled with $Q_B^{-\bullet}$ formation in Photosystem II, *FEBS Lett. 428*, 123−126.
13. Koike, H., and Inoue, Y. (1987) Temperature Dependence of the S-State Transitions in a Thermophilic Cyanobacterium Measured by Thermoluminescence, in *Progress in Photosynthesis Research* (Biggins, J., Ed.) Vol. I, pp 645−648, Martinus Nijhoff, Dordrecht, The Netherlands.
14. Styring, S., and Rutherford, A. W. (1988) Deactivation kinetics and temperature dependence of the S-state transitions in the oxygen-evolving system of Photosystem II measured by EPR spectroscopy, *Biochim. Biophys. Acta 933*, 378−387.
15. Gleiter, H. M., Haag, E., Inoue, Y., and Renger, G. (1993) New results on the functional properties of a photosystem II core complex preparation from spinach, *Photosynth. Res. 35*, 41−53.
16. Kaminskaya, O., Renger, G., and Shuvalow, V. A. (2003) Effect of dehydration on light induced reactions in Photosystem II: photoreactions of cytochrome b559, *Biochemistry 42*, 8119−8132.
17. Noguchi, T., and Sugiura, M. (2002) Flash-induced FTIR difference spectra of the water oxidizing complex in moderately hydrated Photosystem II core films: effect of hydration extent on S-state transitions, *Biochemistry 41*, 2322−2330.
18. Clayton, R. K. (1978) Effects of dehydration on reaction centers from *Rhodopseudomonas sphaeroides*, *Biochim. Biophys. Acta 504*, 255−264.
19. Nikolaev, G. M., Knox, P. P., Kononenko, A. A., Grishanova, N. P., and Rubin, A. B. (1980) Photo-induced electron transport and water state in *Rhodospirillum rubrum* chromatophores, *Biochim. Biophys. Acta 590*, 194−201.
20. Palazzo, G., Mallardi, A., Hochkoeppler, A., Cordone, L., and Venturoli, G. (2002) Electron transfer kinetics in photosynthetic reaction centers embedded in trehalose glasses: trapping of conformational substates at room temperature, *Biophys. J. 82*, 558−568.
21. Berg, A. I., Knox, P. P., Kononenko, A. A., Frolov, E. N.., Khrymova, I. N., Rubin, A. B., Likhtenstein, G. I., Goldansky, V. I., Parak, F., Bukl, M., and Mössbauer, R. (1979) Conformational regulation of the functional activity of photosynthetic membranes of purple bacteria, *Mol. Biol. 13*, 81−89.
22. Parak, F., Frolov, E. N., Kononenko, A. A., Mössbauer, R., Goldansky, V. I., and Rubin, A. B. (1980) Evidence for a correlation between the photoinduced electron transfer and dynamic properties of the chromatophore membranes from *Rhodospirillum rubrum*, *FEBS Lett. 17*, 368−372.
23. Mc Mahon, B. H., Müller, J. D., Wraight, C. A., and Nienhaus, G. U. (1998) Electron transfer and protein dynamics in the photosynthetic reaction center, *Biophys. J. 74*, 2567−2587.
24. Fitter, J., Lechner, R. E., and Dencher, N. A. (1999) Interactions of hydration water and biological membranes studied by neutron scattering, *J. Phys. Chem. B 103*, 8036−8050.
25. Gabel, F., Bicout, D., Lehnert, U., Tehei, M., Weik, M., and Zaccai, G. (2002) Protein dynamics studied by neutron scattering, *Q. Rev. Biophys. 35*, 327−367.
26. Kneller, G. (2005) Quasielastic neutron scattering and relaxation processes in proteins: analytical and simulation-based models, *Phys. Chem. Chem. Phys. 7*, 2641−2655.
27. Smith, J. C. (1991) Protein dynamics: comparison of simulations with inelastic neutron scattering experiments, *Q. Rev. Biophys. 24*, 1−65.

28. Middendorf, H. D., Hayward, R. L., Parker, S. F., Bradshaw, J., and Miller, A. (1995) Vibrational neutron spectroscopy of collagen and model polypeptides. *Biophys. J. 69*, 660−673.
29. Doster, W., Cusack, S., and Petry, W. (1989) Dynamical transition of myoglobin revealed by inelastic neutron scattering, *Nature 337*, 754−756.
30. Natali, F., Relini, A., Gliozzi, A., Rolandi, R., Cavatorta, P., Deriu, A., Fasano, A., and Riccio, P. (2004) The influence of the lipid−protein interaction on the membrane dynamics, *Physica B 350*, 623−626.
31. Paciaroni, A., Orecchini, A., Cinelli, S., Onori, G., Lechner, R. E., and Pieper, J. (2003) Protein dynamics on the picosecond timescale as affected by the environment: a quasielastic neutron scattering study, *Chem. Phys. 292*, 397−404.
32. Fitter, J. (1999) The temperature dependence of internal molecular motions in hydrated and dry alpha-amylase: the role of hydration water in the dynamical transition of proteins, *Biophys. J. 76*, 1034−1042.
33. Cordone, L., Ferrand, M., Vitrano, E., and Zaccai, G. (1999) Harmonic behavior of trehalose-coated carbon-monoxy-myoglobin at high temperature, *Biophys. J. 76*, 1043−1047.
34. Tsai, A. M., Neumann, D. A., and Bell, L. N. (2000) Molecular dynamics of solid-state lysozyme as affected by glycerol and water: a neutron scattering study, *Biophys. J. 79*, 2728−2732.
35. Paciaroni, A., Cinelli, S., and Onori, G. (2002) Effect of the environment on the protein dynamical transition: a neutron scattering study, *Biophys. J. 83*, 1157−1164.
36. Marconi, M., de Francesco, A., Cornicchi, E., Onori, G., and Paciaroni, A. (2005) Hydration and temperature dependent dynamics of lysozyme in glucose-water matrices. A neutron scattering study, *Chem. Phys. 317*, 274−281.
37. Caliskan, G., Briber, R. M., Thirumalai, D., Garcia-Sakai, V., Woodson, S. A., and Sokolov, A. P. (2006) Dynamic transition in tRNA is solvent induced, *J. Am. Chem. Soc. 128*, 32−33.
38. Dellerue, S., and Bellissent-Funel, M.-C. (2000) Relaxational dynamics of water molecules at protein surfaces, *Chem. Phys. 258*, 315−325.
39. Pieper, J., Charalambopoulou, G., Steriotis, T., Vasenkov, S., Desmedt, A., and Lechner, R. E. (2003) Water diffusion in fully hydrated porcine stratum corneum, *Chem. Phys. 292*, 465−471.
40. Teixeira, J., Bellissent-Funel, M.-C., Chen., S. H., and Dianoux, A. J. (1985) Experimental determination of the nature of diffusive motions of water molecules at low temperatures, *Phys. Rev. A 31*, 1913−1917.
41. Lechner, R. E., Fitter, J., Dencher, N. A., and Hauss, T. Low-energy dynamics and biological function, *Physica B, 385−386*, 835−837.
42. Berthold, D. A., Babcock, G. T., and Yocum, C. F. (1981) A highly resolved, oxygen-evolving photosystem II preparation from spinach thylakoid membranes: EPR and electron-transport properties, *FEBS Lett. 134*, 231−234.
43. Völker, M., Ono, T., Inoue, Y., and Renger, G. (1985) Effect of trypsin on PS II particles. Correlation between Hill-activity, Mn-abundance and peptide pattern, *Biochim. Biophys. Acta 767*, 548−556.
44. Christen, G., Seeliger, A., and Renger, G. (1999) $P680^+$ reduction kinetics and redox transition probability of the water oxidising complex as a function of pH and H/D isotope exchange in spinach thylakoids, *Biochemistry 38*, 6082−6092.
45. Christen, G., and Renger, G. (1999) The role of hydrogen bonds for the multiphasic $P680^+$ reduction by Y_Z in photosystem II with intact oxygen evolution capacity. Analysis of kinetic H/D isotope exchange effects, *Biochemistry 38*, 2068−2077.
46. Renger, G., Eckert, H.-J., Bergmann, A., Bernarding, J., Liu, B., Napiwotzki, A., Reifahrt, F., and Eichler, H.-J. (1995) Fluorescence and spectroscopic studies of exciton trapping and electron transfer in photosystem II of higher plants, *Aust. J. Plant Physiol. 22*, 167−181.
47. Lechner, R. E. (1992) Optimization of the chopper system for the cold-neutron time-of-flight spectrometer NEAT at the HMI-Berlin. *Physica B 180−181*, 973−977.
48. Lechner, R. E., Melzer, R., and Fitter, J. (1996) First QINS results from the TOF-spectrometer NEAT, *Physica B 226*, 86−91.
49. Rufflè, B. (2000) *Fitmo User Manual*, Hahn-Meitner-Institut Berlin, Germany.
50. Lechner, R. E., and Riekel, C. (1983) *Neutron Scattering and Muon Spin Rotation*, Springer-Verlag, Berlin, Germany.
51. Bee, M. (1988) *Quasielastic Neutron Scattering: Principles and Applications in Solid State Chemistry, Biology Materials Science*, Adam & Hilger, Philadelphia, PA.
52. Throughout the article the term energy transfer denotes the energy exchanged between the neutron and the sample. This is a general convention in neutron scattering. This term should not be mixed with excitation energy transfer (EET), i.e., the transfer of electronic excitations between pigments of photosynthetic antennae and reaction center complexes. All energy transfer values are given in units of meV, where 1 meV = 8.006 cm^{-1}.
53. Sears, V. F. (1967) Cold neutron scattering by a molecular liquid. III.-Methane, *Can. J. Phys. 45*, 237−254.
54. Volino, F., and Dianoux, A. (1980) Neutron incoherent scattering law for diffusion in a potential of spherical symmetry, *Mol. Phys. 41*, 271−279.
55. Williams, G., and Watts, D. (1969) Non-symmetrical dielectric relaxation behavior arising from a simple empirical decay function, *Trans. Faraday. Soc. 66*, 80−85.
56. Metzler, R., and Klafter, J. (2000) The random walks guide to anomalous diffusion: a fractional dynamics approach, *Phys. Rep. 339*, 1−77.
57. Hinsen, K., Petrescu, A.-J., Dellerue, S., Bellissent-Funel, M.-C., and Kneller, G. R. (2000) Harmonicity in slow protein dynamics, *Chem. Phys. 261*, 25−37.
58. Kneller, G. R. (2000), Inelastic neutron scattering from damped collective vibrations of macromolecules, *Chem. Phys. 261*, 1−24.
59. Lovesey, S. (1984) in *Theory of Neutron Scattering from Condensed Matter*, p 301, Clarendon Press, Oxford, U.K.
60. Tarvin, J. A., and Passell, L., (1979) Analysis of line shapes observed in the scattering of thermal neutrons from superfluid ^{4}He, *Phys. Rev. B 19*, 1458−1462.
61. Teixeira, J., Bellissent-Funel, M.-C., Chen, S. H., and Dorner, B. (1985), Observation of new short-wavelength collective excitations in heavy water by coherent inelastic neutron scattering, *Phys. Rev. Lett. 54*, 2681−2683.
62. Longeville, S., and Lechner, R. E. (2000) Light- and heavy-water dynamics, *Physica B 276−278*, 183−184.
63. Dunahay, T. G., Staehelin, L. A., Seibert, M., Ogilvie, P. D., and Berg, S. P. (1984) Structural, biochemical and biophysical characterization of four oxygen-evolving photosystem II preparations from spinach, *Biochim. Biophys. Acta 764*, 179−193.
64. Shi, L.-X., and Schröder, W. P. (2004) The low molecular mass subunits of the photosynthetic supracomplex, photosystem II. *Biochim. Biophys. Acta 1608*, 75−96.
65. Dekker, J. P., and Boekema, E. J. (2005) Supramolecular organization of thylakoid membrane proteins in green plants. *Biochim. Biophys. Acta 1706*, 12−39.
66. Lehnert, U., Reat, V., Weik, M., Zaccai, G., and Pfister, C. (1998) Thermal motions in bacteriorhodopsin at different hydration levels studied by neutron scattering, *Biophys. J. 75*, 1945−1952.
67. Fitter, J., Lechner, R. E., Bueldt, G., and Dencher, N. A. (1996) Internal molecular motions of bacteriorhodopsin: hydration-induced flexibility studied by quasielastic incoherent neutron scattering using oriented purple membranes, *Proc. Natl. Acad. Sci. U.S.A. 93*, 7600−7605.
68. Pieper, J., Irrgang, K.-D., Renger, G., and Lechner, R. E. (2004) Density of vibrational states of the light-harvesting complex II of green plants studied by inelastic neutron scattering, *J. Phys. Chem. B 108*, 10556−10565.
69. Pieper, J., Voigt, J., and Small, G. J. (1999) Chlorophyll a Franck-Condon factors and excitation energy transfer, *J. Phys. Chem. B 103*, 2319−2322.
70. Diehl, M., Doster, W., Petry, W., and Schober, H. (1997) Water-coupled low-frequency modes of myoglobin and lysozyme observed by inelastic neutron scattering, *Biophys. J. 73*, 2726−2732.
71. Orecchini, A., Paciaroni, A., Bizzarri, A. R., and Cannistraro, S. (2002) Low-frequency vibrational anomalies in β-lactoglobulin: contribution of different hydrogen classes revealed by inelastic neutron scattering, *J. Phys. Chem. B 106*, 12150−12156.
72. Kurkal, V., Daniel, R. M., Finney, J. L., Tehei, M., Dunn, R. V., and Smith, J. C. (2005) Low-frequency enzyme dynamics as a function of temperature and hydration: a neutron scattering study, *Chem. Phys. 317*, 267−273.
73. Hayward, J. A., Daniel, R. M., Finney, J. L., and Smith, J. C. (2003) Use of computer simulation in the interpretation of elastic neutron scattering in complex molecular systems: a small protein in various environments, *Chem. Phys. 292*, 389−396.

74. Steinbach, P. J., Loncharich, R. J., and Brooks, B. R. (1991) The effects of environment and hydration on protein dynamics: a simulation study of myoglobin, *Chem. Phys. 158*, 383−394.
75. Kurkal, V., and Smith, J. C. (2006) Low-temperature protein dynamics: a simulation analysis of interprotein vibrations and the boson peak at 150 K, *J. Am. Chem. Soc. 128*, 2356−2364.
76. Roh, J. H., Novikov, V. N., Gregory, R. B., Curtis, J. E., Chowdhuri, Z., and Sokolov, A. P. (2005) Onsets of anharmonicity in protein dynamics, *Phys. Rev. Lett. 95*, 038101.
77. Curtis, J. E., Tarek, M., and Tobias, D. J. (2004) Methyl group dynamics as a probe of the protein dynamical transition, *J. Am. Chem. Soc. 126*, 15928−15929.
78. Pieper, J., Schödel, R., Irrgang, K.-D., Voigt, J., and Renger, G. (2001) Electron-phonon coupling in solubilized LHC II complexes of green plants investigated by line-narrowing and temperature dependent fluorescence spectroscopy, *J. Phys. Chem. B 105*, 7115−7124.
79. Pieper, J., Rätsep, M., Jankowiak, R., Irrgang, K.-D., Voigt, J., Renger, G., and Small, G. J. (1999) Q_y-level structure and dynamics of solubilized light-harvesting complex II of green plants: pressure and hole burning studies, *J. Phys. Chem. A 103*, 2412−2421.
80. Rogl, H., Schödel, R., Lokstein, H., Kühlbrandt, W., and Schubert, A. (2002) Assignment of spectral substructures to pigment-binding sites in higher plant light-harvesting complex LHC-II, *Biochemistry 41*, 2281−2287.
81. Wu, H.-M., Rätsep, M., Jankowiak, R., Cogdell, R. J., and Small, G. J. (1997) Comparison of the LH2 antenna complexes of *Rhodopseudomonas acidophila* (Strain 10050) and *Rhodobacter sphaeroides* by high-pressure absorption, high-pressure hole burning, and temperature-dependent absorption spectroscopies, *J. Phys. Chem. B 101*, 7641−7653.
82. Hayes, J. M., and Small, G. J. (1978) Non-photochemical hole burning and impurity site relaxation processes in organic glasses, *Chem. Phys. 27*, 151−157.
83. Reddy, N. R. S., Lyle, P. A., and Small, G. J. (1992) Applications of spectral hole burning spectroscopies to antenna and reaction center complexes, *Photosynth. Res. 31*, 167−194.
84. Tietz, C., Jelezko, F., Gerken, U., Schuler, S., Schubert, A., Rogl, H., and Wrachtrup, J. (2001) Single molecule spectroscopy on the light-harvesting complex II of higher plants, *Biophys. J. 81*, 556−562.
85. Zanotti, J.-M., Bellissent-Funel, M.-C., and Parello, J. (1999) Hydration-coupled dynamics in proteins studied by neutron scattering and NMR: the case of the typical EF-hand calcium-binding parvalbumin, *Biophys. J. 76*, 2390−2411.
86. Stowell, M. H. B., McPhilips, T. M., Rees, D. C., Soltis, S. M., Abresch, E., and Feher, G. (1997) Light-induced structural changes in photosynthetic reaction center: implications for mechanism of electron-proton transfer, *Science 276*, 812−816.
87. Xu, Q., Baciou, L., Sebban, P., and Gunner, M. R. (2002) Exploring the energy landscape for Q_A^- to Q_B electron transfer in bacterial photosynthetic reaction centers, *Biochemistry 41*, 10021−10025.
88. Remy, A., and Gerwert, K. (2003) Coupling of light-induced electron transfer to proton uptake in photosynthesis, *Nature Struct. Biol. 10*, 637−644.
89. Breton, J. (2004) Absence of large-scale displacement of quinone QB in bacterial photosynthetic reaction centers, *Biochemistry 43*, 3318−3326.
90. Baxter, R. H. G., Ponomarenko, N., Srajer, V., Pahl, R., Moffat, K., and Norris, J. R. (2004) Time-resoved crystallographic studies of light-induced structural changes in the photosynthetic reaction center, *Proc. Natl. Acad. Sci. U.S.A. 101*, 5982−5987.
91. Mulkidjanian, A. Y., Kozlova, M. A., and Cherepanov, D. A. (2005) Ubiquinone reduction in the photosynthetic reaction centre of Rhodobacter sphaeroides: interplay between electron transfer, proton binding and flips of the quinone ring, *Biochem. Soc. Trans. 33*, 845−850.
92. Lancaster, C. R. D. (2007) Structures of Reaction Centers in Anoxygenic Bacteria, in *Primary Processes of Photosynthesis: Basic Principles and Apparatus, Part 2: Reaction Centers/ Photosystems, Electron Transport Chains, Photophosphorylation and Evolution* (Renger, G., Ed.) pp 5−57, Royal Society of Chemistry, Cambridge, U.K.

BI700179S